

# KVSmooth: Mitigating Hallucination in Multi-modal Large Language Models through Key-Value Smoothing

Siyu Jiang<sup>1,\*</sup> Feiyang Chen<sup>1,\*</sup> Xiaojin Zhang<sup>1</sup> Kun He<sup>1,†</sup>

<sup>1</sup> Huazhong University of Science and Technology

{jiangsiyu, chenfeiyang, xiaojinzhang, brooklet60}@hust.edu.cn

## Abstract

Despite the significant progress of Multi-modal Large Language Models (MLLMs) across diverse tasks, hallucination, which corresponds to the generation of visually inconsistent objects, attributes, or relations, remains a major obstacle to their reliable deployment. Unlike pure language models, MLLMs must ground their generation process in visual inputs; However, existing models often suffer from semantic drift during decoding, causing outputs to diverge from visual facts as the sequence length increases. To address this, we propose KVSmooth, a training-free, plug-and-play method that mitigates hallucination by performing attention-entropy-guided adaptive smoothing on hidden states. Specifically, KVSmooth applies an exponential moving average (EMA) to both keys and values in the KV-Cache while dynamically quantifying the sink degree of each token through its attention distribution entropy to adaptively adjust the smoothing strength. Unlike computationally expensive retraining or contrastive decoding methods, KVSmooth operates efficiently during inference without additional training or model modification. Extensive experiments demonstrate that KVSmooth significantly reduces hallucination ( $CHAIR_S$  from 41.8  $\rightarrow$  18.2) while improving overall performance ( $F_1$  score from 77.5  $\rightarrow$  79.2), achieving higher precision and recall simultaneously, whereas prior methods often sacrifice one for the other, thereby validating the effectiveness and generality of our method.

## 1. Introduction

Multi-modal Large Language Models (MLLMs) [1, 18, 23, 43] have achieved remarkable success across various vision-language tasks, including image captioning [29], visual question answering [9], and multi-modal dialogue [31]. Typically, these models adopt an *en-*

*coder-alignment-decoder* framework: a vision encoder extracts visual representations, a lightweight alignment module (e.g., Q-Former [19] or an MLP) maps them into the linguistic space, and a pretrained LLM — further trained with the alignment module — performs reasoning and generation. This architecture effectively integrates visual and textual representations, enabling coherent and contextually grounded text generation while preserving the LLM’s inherent reasoning ability and maintaining computational efficiency. Despite these advances, MLLMs often over-rely on linguistic priors, resulting in **multi-modal hallucination**, the generation of content misaligned with the visual input [10, 24]. Although numerous strategies have been explored to mitigate this issue [2, 3, 5, 6, 13], hallucination remains a major challenge to achieving trustworthy multi-modal reasoning.

To address this issue, we examine its origin from a generation dynamics perspective. Unlike LLMs that rely solely on linguistic context, MLLMs must tightly align each generated token with visual evidence. This creates a fundamental tension: as decoding progresses, the influence of early visual tokens often decays within hidden representations, weakening visual grounding. The resulting **semantic drift** leads the model to produce text that gradually diverges from the image content. We identify two primary challenges:

1. **Long-term visual dependency decay.** Visual cues gradually fade over long decoding horizons, leading the generated text to drift away from the image context.
2. **Cumulative semantic drift.** Small early-generation inaccuracies accumulate over time, progressively amplifying the gap between the generated description and the visual content.

Correspondingly, we have the following three findings: First, through systematic analysis, we observe a clear distinction in logit dynamics: the mean and variance of *true-object* logits exhibit a **monotonic decrease** over the decoding steps, whereas those of *hallucinated-object* logits display a steady increase. We then introduce attention row-entropy to quantify a token’s sink strength, offering a real-time alternative to attention column-sum. Our analy-

\* Equal contribution.

† Corresponding author.

sis reveals that tokens attracting disproportionate attention are characterized by high row-entropy, indicating an over-smoothed aggregation that dilutes critical visual information. Consequently, **row-entropy is positively correlated with hallucination probability**, explaining why sink tokens often act as precursors to hallucination. Macroscopically, sink tokens emerge at major semantic transitions, where the model averages across previous states to leap into a new semantic space. In multi-modal reasoning, such aggressive transitions can easily deviate from the visual context, leading to hallucinations.

Inspired by these findings, we propose **KVSmooth**, a lightweight, training-free, and plug-and-play solution. Our method introduces two key components: (1) **Exponential Moving Average (EMA) Smoothing on KV-Cache**, which applies token-wise EMA smoothing to Key and Value caches to suppress abrupt state changes and curb the variance explosion of hallucinatory logits; (2) **Entropy-guided coefficient adaptation**, which dynamically increases the smoothing strength for high-entropy sink tokens, further mitigates their impact on generation and reduces hallucination.

KVSmooth offers a novel and effective approach to mitigate hallucinations in MLLMs by stabilizing hidden-state dynamics and provides a reliable and practical foundation for safer multi-modal generation. The main contributions are as follows:

- We introduce the concept of *sink degree*, a novel metric defined via attention row-entropy that enables continuous, real-time identification of tokens prone to hallucination.
- We propose KVSmooth, a lightweight and training-free method that employs adaptive EMA smoothing on the KV-Cache. By dynamically adjusting the smoothing strength based on the sink degree, KVSmooth effectively suppresses hidden-state perturbations that lead to hallucinations without compromising generation efficiency.
- Extensive experiments across multiple benchmarks and MLLMs validate the effectiveness and generality of KVSmooth, demonstrating significant gains in reducing hallucinations while maintaining comprehensiveness.

## 2. Related Work

### 2.1. Hallucinations in MLLMs

Existing efforts to mitigate hallucination in MLLMs fall into two main categories. The first fine-tunes models to align with human preferences or ground-truth annotations [13, 22, 26, 36, 38, 41]. For example, POVID [42] uses reinforcement learning with AI-generated feedback and annotated instructions as preferred responses, effectively reducing hallucination through direct preference optimization. However, such methods demand substantial training data and computational resources.

The second stream avoids parameter updates and instead addresses hallucination through decoding strategies [7, 12, 17, 21, 28, 39] or attention reweighting mechanisms [14–16, 25, 32, 40, 41]. Visual contrastive decoding [17] amplifies and removes hallucinated distributions using noise-augmented views. Follow-up studies further extend contrastive decoding by expanding contrastive sets with diffusion-generated images [28], introducing description-conditioned prefixes [7], or adopting layer-aware contrastive strategies [39], all achieving consistent hallucination reduction without retraining.

Attention reweighting methods aim to rebalance cross-modal attention to mitigate modality imbalance. For instance, PAI [25] enhances attention to visual regions, while MiddleLayer [14] adjusts visual attention by integrating information across multiple heads. However, both approaches tend to suppress correctly described objects along with hallucination. To address this, SPARC [15] tracks cross-step attention gaps to detect critical visual tokens and selectively reinforces those whose influence increases over time, thereby slightly reducing hallucinations while maintaining high recall. Meanwhile, TAME [32] identifies hallucination as stemming from polarized variance in attention spectra, where extreme eigenvalues cause over-anchoring on a few tokens. They rescale Query–Key variances to restore attention balance. PruneHal [30] reduces hallucinations by pruning redundant visual tokens on KV-Cache, which re-allocates the model’s attention to important visual tokens. Overall, attention misalignment reveals MLLMs’ chronic under-utilization of visual cues during deep generation.

### 2.2. Attention Sink in MLLMs

The attention sink phenomenon was first identified in StreamingLLM [37], where LLMs consistently assigned disproportionately high attention to the beginning-of-sequence (BOS) token. A recent study [8] provides a geometric explanation: key of the first token lies on a distinct manifold, resulting in small angles with most queries and causing an attention sink, where attention disproportionately focuses.

OPERA [11] generalized this concept beyond BOS, identifying semantically redundant “aggregation tokens” that persistently receive maximal attention across decoding steps. These textual sink tokens absorb substantial attention resources while contributing little factual grounding, and their over-activation correlates strongly with hallucinations—extending the sink notion from a positional artifact to a broader linguistic behavior in auto-regressive decoding.

To mitigate sink-induced hallucinations, methods such as OPERA [11] employ an over-trust logit penalty and retrospection-allocation to revisit and re-evaluate sink tokens. AttnReal [34] redistributes attention from textual sinks toward visual evidence, while FarSight [33] reserves

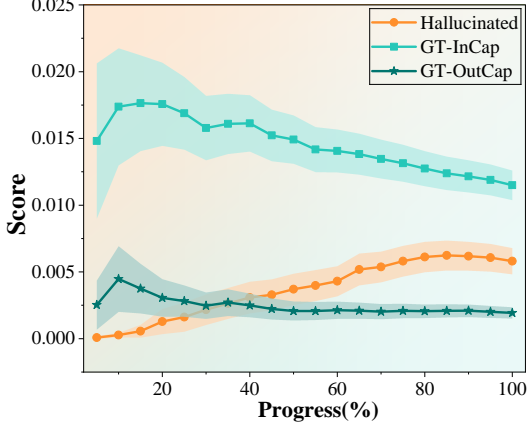


Figure 1. Variation of object logit scores during caption generation. We analyze 200 images and compute the average score of each object category across different generation stages. Objects are categorized into three groups: (1) **GT-InCap** - objects appearing in both the image and the generated caption, (2) **GT-OutCap** - objects present in the image but missing from the caption, and (3) **Hallucinated** - objects mentioned in the caption but absent from the image. The y-axis denotes the average logit score of each object group, while the x-axis represents the generation progress. Each caption is divided into twenty stages by token count, where each stage includes all tokens up to that point. The mean and variance are computed for each stage and 95% confidence intervals are reported.

attention for future context to reduce sink dominance. Though differing in strategy, these approaches share the goal of suppressing or reallocating attention away from sink tokens.

However, existing work primarily focuses on reducing the occurrence of sink tokens or diminishing the attention allocated to the most dominant sink tokens, without explaining why sink tokens trigger hallucinations. In this study, we reveal that aggregation tokens, while integrating context, can distort internal representations during fusion and directly induce hallucinations. Correspondingly, we propose to regularize and correct the hidden states of such tokens, aiming to suppress hallucinations by stabilizing their semantic contributions and enhancing multi-modal factual grounding.

### 3. Observation

In this section, we begin by formulating MLLM generation, and then describe our three key observations in detail.

#### 3.1. Formulation of MLLMs Generation

MLLMs process both images and text. The image is transformed into a sequence of visual tokens  $x^v = \{x_0, x_1, \dots, x_{N-1}\}$ , where  $N$  is typically fixed, while the input text is tokenized into  $x^p = \{x_N, x_{N+1}, \dots, x_{N+M-1}\}$ .

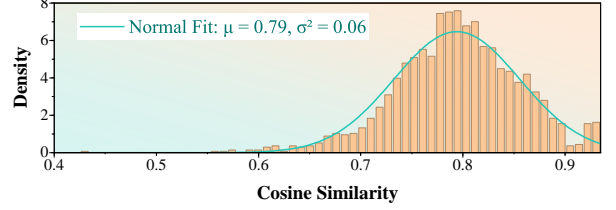


Figure 2. Distribution of cosine similarity between attention row-entropy and column-sum across all layers during the generation process. The similarity values exhibit a precise unimodal distribution centered around 0.79 with low variance, indicating a stable and strong positive correlation between attention row-entropy and column-sum.

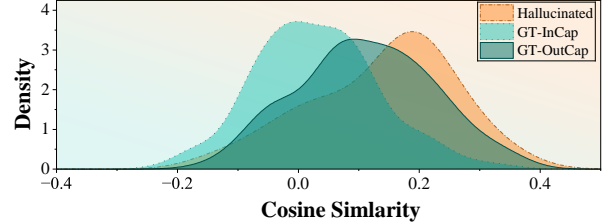


Figure 3. Distribution of cosine similarity between logit ranking and attention row-entropy across object types in 200 images. We compute the cosine similarity between row-entropy and ranking scores for three object categories. Hallucinated objects exhibit the highest similarity, indicating that greater row-entropy correlates with stronger hallucination tendencies, whereas genuine objects (GT-InCap and GT-OutCap) show lower or slightly negative correlations.

These visual and text tokens are concatenated to form the initial input sequence for the decoder.

Generation proceeds auto-regressively. After generating  $k$  tokens, the decoder input is of length  $L = N + M + k$ , denoted as  $\{x_0, x_1, \dots, x_{L-1}\}$ . The model then computes the probability distribution for the next token at position  $t = L$ .

Let  $Q_t^{(l,h)}, K_j^{(l,h)}, V_j^{(l,h)} \in \mathbb{R}^d$  represent the query, key, and value vectors of head  $h$  in layer  $l$ , where  $t = L$  is the current token position, and  $j = 0, 1, \dots, L - 1$  indexes the context. The attention score is:

$$A_{t,j}^{(l,h)} = \frac{(Q_t^{(l,h)})^\top K_j^{(l,h)}}{\sqrt{d}}, \quad (1)$$

and is normalized via softmax over  $j$ :

$$\alpha_{t,j}^{(l,h)} = \frac{\exp(A_{t,j}^{(l,h)})}{\sum_{n=0}^{L-1} \exp(A_{t,n}^{(l,h)})}. \quad (2)$$

The output of head  $h$  is:

$$o_t^{(l,h)} = \sum_{j=0}^{L-1} \alpha_{t,j}^{(l,h)} V_j^{(l,h)}. \quad (3)$$

Outputs from all  $H$  heads are concatenated and projected to form layer- $l$ 's hidden state  $h_t^l$ , which is passed to the next block.

Finally, the hidden state of the last layer is projected to vocabulary logits. The next-token probability is:

$$p_\theta(y_t | v, x, y_{<t}) \propto \exp(\text{logit}_\theta(y_t | v, x, y_{<t})), \quad (4)$$

where  $\text{logit}_\theta(y_t | v, x, y_{<t})$  is the unnormalized logit for  $y_t$ . The next token is sampled from this distribution, and this process repeats.

### 3.2. Divergent Logit Dynamics of Hallucinated vs. Non-Hallucinated Objects

We first examine how the logit distributions of different object categories evolve during decoding. As shown in Figure 1, Ground Truth (GT) objects - comprising both GT-InCap and GT-OutCap - exhibit a monotonic decline in mean logit while their variance stabilizes, indicating that the model's focus on visually grounded cues gradually weakens, causing their scoring advantage to fade over time. In contrast, hallucinated objects display rising mean logits accompanied by slightly increasing variance. This divergence suggests that spurious candidates accumulate instability in hidden representations, making them more likely to be erroneously sampled in later steps. Thus, preserving a stable and dominant signal for GT objects while suppressing the anomalous amplification of hallucinated ones is essential for effective hallucination mitigation.

### 3.3. Row-Entropy Affinity and Attention Sinks

Previous work [11] introduced a column-wise attention score to identify aggregation tokens. However, computing tokens with large attention column-sums requires multiple decoding steps and backtracking, which is computationally inefficient. To address this, we propose attention row-entropy as a real-time metric for quantifying a token's sink strength. Inspired by [8], the BOS token occupies an average angular position in the hidden-state space, naturally exhibiting high cosine similarity with other tokens and, consequently, high attention scores. We hypothesize that aggregation tokens follow a similar pattern.

Formally, we define the attention row-entropy of token  $x_t$  as

$$z_t^l = -\frac{1}{H} \sum_{j=0}^{L-1} \sum_{h=0}^{H-1} \alpha_{t,j}^{(l,h)} \log(\alpha_{t,j}^{(l,h)} + \varepsilon), \quad (5)$$

which serves as a proxy for its aggregation strength.

As shown in Figure 2, tokens with high row-entropy - *i.e.*, diffuse attention distributions - tend to produce hidden states that approximate the historical average, lying near the central manifold of past representations. These tokens thus

exhibit small angular distances to most hidden states and attract disproportionately high attention in subsequent steps, forming attention sinks. Compared to aggregation centered on a few key tokens, global averaging introduces stronger hidden-state distortions that accumulate over time, amplifying hallucinations as subsequent tokens repeatedly attend to these sinks.

### 3.4. Entropy-Ranking Coupling in Hallucinated Objects

While prior studies have linked hallucinations to sink tokens, the underlying mechanism remains unclear. To elucidate this, we analyze the joint evolution of logit rankings and attention row-entropy for hallucinated versus faithful object tokens during generation.

We observe a weak positive correlation between ranking and row-entropy for hallucinated objects: the more uniformly a token attends (*i.e.*, higher entropy), the higher the logits of hallucinated objects tend to rise. GT objects, however, exhibit the opposite trend. This finding reveals a direct link between attention uniformity and hallucination risk: sink tokens, which average across the entire context, systematically inflate hallucinated object scores.

At a broader level, this behavior originates from pre-trained LLMs, which summarize previously observed entities and continuously introduce new entities during generation. When fine-tuned into MLLMs, this tendency persists: repeated high-entropy aggregations continuously amplify spurious object scores, allowing them to dominate the output.

### 3.5. Summary of Insights

In summary, our analysis identifies variance propagation via sink tokens as the root cause of object hallucination. **Obs1** reveals that hallucination scores increase while GT scores decay over time. **Obs2** demonstrates that attention row-entropy strongly correlates with aggregation (sink) behavior. **Obs3** establishes the causal coupling between attention row-entropy and hallucination amplification. Together, these findings motivate a variance-regularized state-evolution framework aimed at (1) maintaining GT object dominance and (2) suppressing hallucination-inducing stochastic fluctuations from sink tokens.

## 4. Methodology

In this section, we begin by deriving an Exponential Moving Average (EMA)-based smoothing strategy following **Obs1**. Both theoretical analysis and empirical results show that applying EMA to the key and value is most effective, forming our EMA Smoothing on KV-Cache method (Section 4.1). Then, inspired by **Obs2** and **Obs3**, we introduce an adaptive coefficient selection mechanism guided by attention entropy, which applies stronger smoothing to tokens

with higher sink tendencies, termed Entropy-Guided Coefficient Adaptation (Section 4.2).

#### 4.1. EMA Smoothing on KV-Cache

As encouraged by **Obs1**, the mean and variance of the hallucination object logit anomaly increase, indicating that the standard decoding process lacks the  $p(h_t|h_{<t})$  constraint. To keep the decoding trajectory ideally smooth, we formalize the following hypothesis:

$$h_t = h_{t-1} + \epsilon_t, \epsilon_t \sim N(0, \sigma_p^2). \quad (6)$$

Consequently, the transition prior is

$$P(h_t|h_{t-1}) = N(h_t; h_{t-1}, \sigma_p^2) \propto \exp\left(-\frac{1}{2\sigma_p^2}\|h_t - h_{t-1}\|^2\right). \quad (7)$$

Under this prior, the maximum-a-posteriori (MAP) estimate of  $h_t$  is given by

$$\hat{h}_t = \operatorname{argmax}_{h_t} \left[ \underbrace{\log P(o_t|h_t)}_{\text{likelihood}} + \underbrace{\log P(h_t|h_{t-1})}_{\text{smoothed prior}} \right], \quad (8)$$

where  $o_t$  denotes the raw hidden state observed at step  $t$ . Assuming both terms follow Gaussian distributions,

$$\hat{h}_t = \operatorname{argmax}_{h_t} \left[ -\frac{1}{2\sigma_o^2}\|o_t - h_t\|^2 - \frac{1}{2\sigma_p^2}\|h_t - h_{t-1}\|^2 \right]. \quad (9)$$

Taking the derivative of (9) with respect to  $h_t$ , setting it to zero, and solving for  $\hat{h}_t$  yields

$$\hat{h}_t = \frac{\sigma_p^2}{\sigma_p^2 + \sigma_o^2} o_t + \frac{\sigma_o^2}{\sigma_p^2 + \sigma_o^2} h_{t-1}. \quad (10)$$

Defining

$$\lambda_t = \frac{\sigma_o^2}{\sigma_p^2 + \sigma_o^2}, \quad (11)$$

the estimate simplifies to an exponential moving average (EMA) form:

$$\hat{h}_t = (1 - \lambda_t) o_t + \lambda_t h_{t-1}. \quad (12)$$

Thus, when the likelihood follows Gaussian in  $h_t$ , the MAP estimator coincides exactly with an exponential moving average. The detailed derivation can be found in Appendix A.

Motivated by this equivalence, we apply an EMA update directly to the current hidden state  $h_t$ . This operation constitutes an efficient, closed-form instantiation of the Bayesian-optimal smoother, optimally balancing fidelity to the current observation with temporal consistency.

Another question arises: how exactly should we smooth  $h_t$ , and at which stage should this be applied? Empirically,

we find that simultaneously updating the key  $K_t$  and value  $V_t$  stored in the preceding KV-Cache, rather than the raw hidden variable itself, could maximally suppress both mean and variance of the logits. Section 3.1 has shown how  $K_t$  and  $V_t$  yield the hidden state  $h_t$ . By simultaneously smoothing  $K_t$  and  $V_t$  so that each satisfies the distribution in Eq. (6), and exploiting the fact that the product of two independent Gaussian distributions remains Gaussian, we conclude that the resulting product  $h_t$  also obeys the same distribution.

By operating on the KV-Cache, a larger smoothing coefficient could be applied, achieving the most substantial regularization effect on the logits and consequently yielding the most effective hallucination suppression. The experiments in Section 5.4.1 further validate the effectiveness of smoothing  $K_t$  and  $V_t$ , while Appendix D.2 investigates the optimal layers for applying such smoothing.

#### 4.2. Entropy-Guided Coefficient Adaptation

Prior work has shown that sink tokens are more likely to trigger hallucinations. As revealed in **Obs2**, the traditional column-sum metric used to identify sink tokens is positively correlated with our proposed row-entropy: higher row-entropy indicates a greater likelihood that a token acts as a sink token and induces hallucination. Therefore, it is crucial to attenuate the influence of high-entropy tokens during subsequent generation steps.

In EMA smoothing, the coefficient directly controls the smoothing strength: a larger coefficient yields stronger smoothing, thereby reducing the token’s impact on future updates. By adaptively modulating this coefficient, we can suppress high row-entropy tokens. However, determining the optimal coefficient is non-trivial. Since  $\sigma_o^2$  is unavailable, the overall smoothing coefficient  $\lambda_t$  remains intractable. Using a uniform smoothing coefficient for all tokens may also over-suppress the semantic flow of normal tokens, ultimately degrading recall.

Inspired by **Obs3**, we believe that different tokens contribute unequally to hallucination based on their row-entropy-ranking. We aim to introduce a scalar that can dynamically provide feedback on each token’s contribution to hallucination during the generation process.

Specifically, at time step  $t$ , we first compute the row-entropy  $z_t^l$  of token  $x_t$  for layer  $l$  following Eq. (5). We maintain a First-In-First-Out queue  $S^l = z_{t-M+1}^l, \dots, z_t^l$ , where  $M$  denotes the maximum length of the queue. The queue preserves the temporal order of tokens. We assume that the growth of sequence length  $L$  during generation has a negligible effect on the computation of row-entropy within the queue. After inserting  $z_t^l$  into the queue, we compute its percentile rank  $k$ , *i.e.*, the count of elements in the queue with row-entropy smaller than  $z_t^l$ , regardless of their positions in the queue. We then calculate the proportion of

these elements within the queue and use this value as the smoothing coefficient  $\hat{\lambda}_t^l$  for token  $x_t$  at layer  $l$ . Formally,  $\hat{\lambda}_t^l$  is defined as:

$$\hat{\lambda}_t^l = \frac{k}{M} \in \left[0, \frac{M-1}{M}\right]. \quad (13)$$

Furthermore, to preserve information from earlier hidden states while retaining the intrinsic property of each current state, we clip extremely large or small values of  $\hat{\lambda}_t^l$ . Concretely, we define a hyperparameter  $\lambda_{\text{ref}}$  to guide the truncation and perform the clipping as:

$$\tilde{\lambda}_t^l = \max\left(\lambda_{\text{ref}} - 0.2, \min\left(\lambda_{\text{ref}} + 0.2, \hat{\lambda}_t^l\right)\right), \quad (14)$$

which constrains  $\hat{\lambda}_t^l$  within a narrow window around itself, stabilizing generation while preserving representational diversity.

### 4.3. The Final KVSmooth Method

We designate a subset of decoder layers in the MLLM as smoothing targets. At generation step  $t$ , for each target layer  $l$ , we compute the token-specific smoothing strength  $\hat{\lambda}_t^l$  using attention-row-entropy-based adaptive coefficient selection. The KV-Cache of token  $x_t$  on layer  $l$  is then updated via EMA smoothing:

$$\begin{aligned} \hat{K}_t^l &= (1 - \tilde{\lambda}_t^l)K_t^l + \tilde{\lambda}_t^l K_{t-1}^l, \\ \hat{V}_t^l &= (1 - \tilde{\lambda}_t^l)V_t^l + \tilde{\lambda}_t^l V_{t-1}^l. \end{aligned} \quad (15)$$

Applying KVSmooth effectively suppresses the mean and variance of logit probabilities associated with hallucinatory objects by reducing the emergence of sink tokens. By keeping the decoder anchored to visual priors, KVSmooth prevents abrupt state deviations from image-grounded evidence, thereby mitigating hallucination. Further algorithmic details are provided in Appendix E. Notably, KVSmooth is lightweight, training-free, and can be seamlessly integrated in a plug-and-play manner.

## 5. Experiments

### 5.1. Experimental Setup

**Baselines.** We compare our method with five representative training-free approaches. VCD [17] is a typical contrastive decoding method that enhances the influence of visual information. OPERA [11] mitigates hallucination by reducing sink-token effects through over-trust penalty and retrospection-based decoding. We also include three attention-redistribution methods: PAI [25], SPARC [15], and MiddleLayer [14], which enhance visual attention.

**Implementation Details.** We evaluate our method on three representative MLLMs: LLaVA-1.5 [23], MiniGPT-

4 [43], and InstructBLIP [18] to assess both effectiveness and generalization. All models adopt their 7B versions. Experiments are conducted on four standard hallucination benchmarks: CHAIR [29] for caption hallucination; OPOPE [4] for object presence verification; AMBER [35] for comprehensive multi-scenario evaluation; and Object HalBench [29] evaluates object hallucination by leveraging GPT [27] to assist in object extraction. All models perform greedy decoding with a maximum of 512 generated tokens. Our method applies EMA smoothing to layers 3–31 across all models, using a fixed FIFO queue of length 15. The reference hyperparameter  $\lambda_{\text{ref}}$  is set to 0.9, 0.5, and 0.7 for LLaVA-1.5, MiniGPT-4, and InstructBLIP, respectively, and this configuration is applied consistently across all benchmark evaluations.

### 5.2. Main Results on CHAIR

Table 1 presents the quantitative results on the CHAIR benchmark across three representative LVLMS. Overall, our method strikes an effective balance between hallucination suppression and coverage of real objects. In particular, for LLaVA-1.5, the CHAIR<sub>S</sub> decreases from 41.8 to 18.2, corresponding to a relative reduction of approximately 56%. On MiniGPT-4 and InstructBLIP, our approach consistently achieves the lowest CHAIR<sub>S</sub> values, confirming its robustness and effectiveness.

Moreover, across all models, our approach achieves the highest or second-highest F<sub>1</sub> values while significantly reducing hallucinations, showing that it effectively suppresses spurious objects without sacrificing faithful description quality. To further investigate this trade-off, we conduct detailed analyses on two aspects: the precision–recall trade-off and the CHAIR<sub>S</sub>–F<sub>1</sub> trade-off.

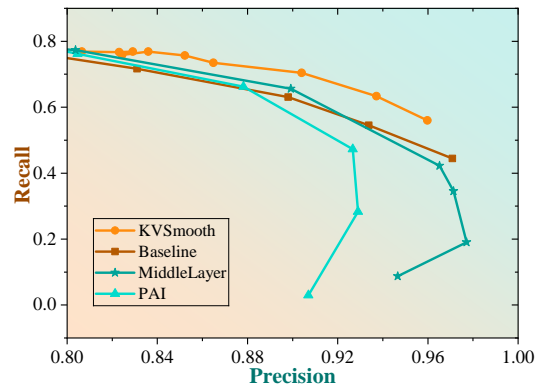


Figure 4. Precision–recall trade-off on LLaVA-1.5 (CHAIR benchmark). Curves nearer the top-right corner denote superior overall performance. KVSmooth attains a strong precision–recall balance, clearly surpassing all competing methods.

**Analysis on Precision-Recall Trade-off.** We further analyze model performance using Precision-Recall (PR)

Table 1. CHAIR performance of different models. Lower CHAIR<sub>S</sub> and higher F<sub>1</sub> indicate better performance. The best results in each column are highlighted in **bold**, and the second-best are underlined.

Method	LLaVA-1.5		MiniGPT-4		InstructBLIP	
	CHAIR <sub>S</sub> ↓	F <sub>1</sub> ↑	CHAIR <sub>S</sub> ↓	F <sub>1</sub> ↑	CHAIR <sub>S</sub> ↓	F <sub>1</sub> ↑
Baseline	41.8	77.5	31.8	69.9	61.4	71.6
PAI	22.6	75.5	24.6	71.0	63.4	71.1
OPERA	44.2	78.6	27.4	69.4	68.0	69.2
VCD	56.0	71.1	31.0	70.0	61.6	71.6
SPARC	45.6	78.9	26.8	<b>72.5</b>	70.0	70.0
MiddleLayer	<b>17.8</b>	75.9	24.6	71.2	75.0	67.2
Ours (w/o Ada.)	36.2	<b>79.2</b>	<u>23.0</u>	71.3	<u>47.8</u>	<u>74.1</u>
Ours	<u>18.2</u>	<b>79.2</b>	<b>17.0</b>	<u>71.7</u>	<b>42.2</b>	<b>75.1</b>

Table 2. OPOPE performance of different models. Higher Accuracy (*Acc*), Precision (*Pre*), and F<sub>β=0.2</sub> indicate better object presence recognition and hallucination mitigation. The best results in each column are highlighted in **bold**, and the second-best are underlined.

Method	LLaVA-1.5			MiniGPT-4			InstructBLIP		
	Acc ↑	Pre ↑	F <sub>β=0.2</sub> ↑	Acc ↑	Pre ↑	F <sub>β=0.2</sub> ↑	Acc ↑	Pre ↑	F <sub>β=0.2</sub> ↑
Baseline	76.75	86.17	85.03	67.94	87.43	83.94	73.94	83.26	82.06
PAI	70.95	89.39	86.47	67.65	88.43	84.60	73.69	82.30	81.19
OPERA	<b>77.92</b>	86.86	85.81	67.65	88.85	84.93	73.03	81.93	80.76
VCD	73.57	83.98	82.59	67.86	87.39	83.88	74.23	<u>83.51</u>	82.31
SPARC	<u>77.04</u>	86.13	85.04	<u>68.08</u>	88.37	84.72	<u>74.57</u>	82.87	81.84
MiddleLayer	70.97	<u>89.43</u>	<u>86.51</u>	<u>68.08</u>	<u>89.61</u>	<u>85.69</u>	<b>77.14</b>	83.13	<u>82.44</u>
Ours	74.60	<b>91.20</b>	<b>88.90</b>	<b>68.13</b>	<b>90.74</b>	<b>86.59</b>	73.89	<b>85.19</b>	<b>83.69</b>

curves under the CHAIR benchmark (Figure 4). Precision measures the model’s ability to avoid hallucinations, while recall captures its ability to cover Ground Truth (GT) objects. We compare the baseline, two representative attention-reallocation methods, and our approach by sweeping their key parameters: the number of generated sentences (Baseline), the enhancement coefficient for visual tokens (PAI and MiddleLayer), and the EMA decay rate  $\lambda_{\text{ref}}$  (KVSmooth). A larger area under the PR curve indicates a better balance between hallucination suppression and object coverage. Our method consistently achieves superior PR curves across all models, maintaining high precision with high recall. In contrast, while other methods can improve precision, they often result in significant recall degradation—sometimes even falling below the baseline at comparable precision levels.

**Analysis on CHAIR<sub>S</sub>-F<sub>1</sub> Trade-off.** We further explore the relationship between CHAIR<sub>S</sub> and F<sub>1</sub> using the same parameter sweep settings as the precision–recall trade-off. Figure 5 shows that other methods tend to suffer a significant drop in F<sub>1</sub> when reducing CHAIR<sub>S</sub>, whereas our approach can substantially reduce CHAIR<sub>S</sub> while maintaining F<sub>1</sub> almost unchanged. This advantage stems from our adaptive mechanism (Section 4.2), which precisely identifies sink tokens that require smoothing and selectively mitigates hallucinations without affecting GT object de-

Table 3. Amber and Object HalBench performance of different models. Lower CHAIR (*C*), CHAIR<sub>S</sub> (*C<sub>S</sub>*), CHAIR<sub>SR</sub> (*C<sub>SR</sub>*), CHAIR<sub>I</sub> (*C<sub>I</sub>*), *Hal*, and *Cog* indicate better hallucination mitigation, while higher *Cover* (*Cov*) and *CoCoNum* (*Num*) indicate better object coverage. The best results for each metric are highlighted in **bold**.

Model	Method	Amber				Object HalBench			
		<i>C</i> ↓	<i>Cov</i> ↑	<i>Hal</i> ↓	<i>Cog</i> ↓	<i>C<sub>S</sub></i> ↓	<i>C<sub>SR</sub></i> ↓	<i>C<sub>I</sub></i> ↓	<i>Num</i> ↑
LLaVA-1.5	Baseline	6.1	50.6	27.3	2.8	48.1	45.3	24.7	283
	Ours	<b>3.1</b>	<b>50.8</b>	<b>18.7</b>	<b>1.3</b>	<b>17.5</b>	<b>16.7</b>	<b>9.0</b>	<b>286</b>
MiniGPT-4	Baseline	<b>15.3</b>	<b>63.3</b>	65.3	11.0	27.5	26.3	14.5	<b>287</b>
	Ours	17.8	59.5	<b>39.6</b>	<b>5.1</b>	<b>15.8</b>	<b>15.7</b>	<b>8.6</b>	279
InstructBLIP	Baseline	14.7	<b>58.8</b>	65.8	9.8	39.6	37.7	21.1	<b>287</b>
	Ours	<b>5.4</b>	57.6	<b>43.7</b>	<b>5.7</b>	<b>23.7</b>	<b>22.0</b>	<b>13.3</b>	278

Table 4. Performance comparison under different smoothing methods. Lower CHAIR<sub>S</sub> (*C<sub>s</sub>*) indicates better hallucination mitigation, and higher F<sub>1</sub> indicates better overall performance. The best results in each column are highlighted in **bold**, and the second-best are underlined.

Method	LLaVA-1.5		MiniGPT-4		InstructBLIP	
	<i>C<sub>s</sub></i> ↓	F <sub>1</sub> ↑	<i>C<sub>s</sub></i> ↓	F <sub>1</sub> ↑	<i>C<sub>s</sub></i> ↓	F <sub>1</sub> ↑
Attention output ( <i>o<sub>t</sub></i> )	<u>33.8</u>	74.7	<u>19.8</u>	66.5	84.4	61.2
Key ( <i>K<sub>t</sub></i> )	35.6	<b>79.4</b>	24.0	<u>70.6</u>	<u>73.2</u>	<u>70.2</u>
Key-Value ( <i>K<sub>t</sub>, V<sub>t</sub></i> )	<b>18.2</b>	<u>79.2</u>	<b>17.0</b>	<b>71.7</b>	<b>42.2</b>	<b>75.1</b>

scriptions. In addition, Appendix C further reports the sensitivity analysis of the hyperparameter for KVSmooth, as well as the analysis of the CHAIR<sub>S</sub>-F<sub>1</sub> trade-off on the other two models. Besides, we provide additional qualitative generation examples in Appendix F and include an efficiency analysis in Appendix B, which shows that KVSmooth maintains inference speed and memory usage close to the baseline while incurring substantially lower overhead than competing methods.

### 5.3. Generalization Experiments

To further verify the generalization ability of our approach beyond the CHAIR benchmark, we extend the evaluation to

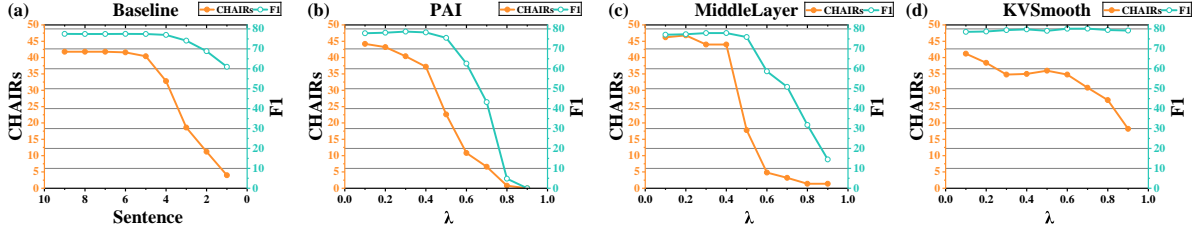


Figure 5. Sensitivity analysis of the hyperparameter  $\lambda_{\text{ref}}$  for KVSmooth based on LLaVA-1.5 and comparisons of four methods in terms of the CHAIR<sub>S</sub>-F<sub>1</sub> trade-off (CHAIR benchmark). It is evident that larger values of  $\lambda_{\text{ref}}$  lead to stronger smoothing and improved hallucination mitigation. Moreover, our method consistently maintains the balance between precision and recall, demonstrating stability and reliability across different smoothing strengths.

three complementary hallucination benchmarks—**OPOPE**, **AMBER**, and **Object HalBench**—which jointly assess object presence verification, multi-scenario hallucination robustness, and GPT-assisted object grounding.

**OPOPE.** As shown in Table 2, our method achieves the highest average Accuracy and  $F_{\beta=0.2}$  across random, popular, and adversarial object sets, demonstrating strong hallucination mitigation in all three scenarios.

**AMBER.** As shown in Table 3, it can be observed that our method substantially reduces hallucinated objects while retaining coverage of GT objects. Specifically, for LLaVA-1.5, our approach not only yields a remarkable reduction in CHAIR and *Hal* (fewer hallucinations) but also slightly increases *Cover*, with more GT objects correctly described while suppressing hallucinations. For MiniGPT-4 and InstructBLIP, our method also consistently lowers hallucination metrics compared to the baseline while maintaining competitive coverage of real objects.

**Object HalBench.** As shown in Table 3, KVSmooth significantly decreases the sentence-level hallucination rate CHAIR<sub>SR</sub> by 63.1%, 40.3%, and 41.6% for LLaVA-1.5, MiniGPT-4, and InstructBLIP, respectively. These consistent improvements across all metrics confirm the effectiveness and generalizability of our approach in mitigating multi-modal hallucinations under varied evaluation protocols.

## 5.4. Ablation Study

### 5.4.1. Effect of Smoothing Method

To determine the optimal positions for applying EMA updates, we investigate the impact of updating different internal states on hallucination mitigation. Specifically, EMA is applied separately to the key  $K_t$ , the attention output  $o_t$ , and jointly to both key and value ( $K_t, V_t$ ). Their performance is evaluated in terms of CHAIR<sub>S</sub> and F<sub>1</sub> scores on the CHAIR benchmark, as summarized in Table 4.

From the results, it can be seen that applying EMA solely to the key vectors is less effective than updating both key and value vectors simultaneously. In contrast, applying EMA directly to the hidden states leads to a severe drop

in recall, indicating a significant reduction in the model’s ability to retain correct object information. These findings suggest that joint EMA updates on the key and value vectors strike the best balance, effectively mitigating hallucinations while preserving faithful object descriptions.

### 5.4.2. Module Ablation

Our method comprises two main components: (1) EMA smoothing on KV-Cache (Section 4.1) and (2) entropy-guided coefficient adaptation (Section 4.2).

To evaluate the contribution of the adaptive design, we set the EMA update coefficient  $\lambda$  as a constant and select the value that yields the highest F<sub>1</sub> score for comparison. As shown in Table 1, even with the best constant  $\lambda$ , our adaptive mechanism still outperforms it. This demonstrates that the adaptive design can precisely identify tokens more likely to induce hallucinations and apply stronger smoothing to them. In contrast, a fixed  $\lambda$  may over-smooth genuine object regions or under-smooth hallucinated ones, thereby limiting the model’s ability to generate accurate and detailed descriptions.

## 6. Conclusion

This work investigated the critical issue of hallucination in multi-modal models, with a specific focus on semantic drift during long text generation. We established three pivotal observations: **Obs1** reveals that both the mean and variance of logit scores for hallucinated objects progressively increase during generation; **Obs2** identifies a strong correlation between attention row-entropy and attention aggregation patterns; and **Obs3** demonstrates a causal coupling between attention row-entropy and hallucination amplification. Leveraging these insights, we proposed KVSmooth, a lightweight, training-free, and plug-and-play approach that dynamically computes row-entropy during generation and applies adaptive EMA smoothing to the Key and Value vectors. Extensive experiments validate that KVSmooth not only achieves state-of-the-art performance in mitigating hallucinations but also preserves comprehensive and accurate coverage of real objects.

## References

- [1] Shuai Bai, Keqin Chen, Xuejing Liu, Jialin Wang, Wenbin Ge, Sibao Song, Kai Dang, Peng Wang, Shijie Wang, Jun Tang, et al. Qwen2. 5-vl technical report. *arXiv preprint arXiv:2502.13923*, 2025. 1
- [2] Junzhe Chen, Tianshu Zhang, Shiyu Huang, Yuwei Niu, Linfeng Zhang, Lijie Wen, and Xuming Hu. Ict: Image-object cross-level trusted intervention for mitigating object hallucination in large vision-language models. In *Proceedings of the Computer Vision and Pattern Recognition Conference*, pages 4209–4221, 2025. 1
- [3] Xuweiyi Chen, Ziqiao Ma, Xuejun Zhang, Sihan Xu, Shengyi Qian, Jianing Yang, David Fouhey, and Joyce Chai. Multi-object hallucination in vision language models. *Advances in Neural Information Processing Systems*, 37:44393–44418, 2024. 1
- [4] Zhaorun Chen, Zhuokai Zhao, Hongyin Luo, Huaxiu Yao, Bo Li, and Jiawei Zhou. Halc: Object hallucination reduction via adaptive focal-contrast decoding. *arXiv preprint arXiv:2403.00425*, 2024. 6, 1, 2
- [5] Yeongjae Cho, Keonwoo Kim, Taebaek Hwang, and Sungzoon Cho. Do you keep an eye on what i ask? mitigating multimodal hallucination via attention-guided ensemble decoding. *arXiv preprint arXiv:2505.17529*, 2025. 1
- [6] Alessandro Favero, Luca Zancato, Matthew Trager, Siddharth Choudhary, Pramuditha Perera, Alessandro Achille, Ashwin Swaminathan, and Stefano Soatto. Multi-modal hallucination control by visual information grounding. In *IEEE/CVF Conference on Computer Vision and Pattern Recognition, CVPR 2024, Seattle, WA, USA, June 16-22, 2024*, pages 14303–14312. IEEE, 2024. 1
- [7] Sreyan Ghosh, Chandra Kiran Reddy Evuru, Sonal Kumar, Utkarsh Tyagi, Oriol Nieto, Zeyu Jin, and Dinesh Manocha. Visual description grounding reduces hallucinations and boosts reasoning in vlms. In *The Thirteenth International Conference on Learning Representations, ICLR 2025, Singapore, April 24-28, 2025*. OpenReview.net, 2025. 2
- [8] Xiangming Gu, Tianyu Pang, Chao Du, Qian Liu, Fengzhuo Zhang, Cunxiao Du, Ye Wang, and Min Lin. When attention sink emerges in language models: An empirical view. In *The Thirteenth International Conference on Learning Representations, ICLR 2025, Singapore, April 24-28, 2025*. OpenReview.net, 2025. 2, 4
- [9] Jiaxian Guo, Junnan Li, Dongxu Li, Anthony Meng Huat Tiong, Boyang Li, Dacheng Tao, and Steven Hoi. From images to textual prompts: Zero-shot visual question answering with frozen large language models. In *Proceedings of the IEEE/CVF conference on computer vision and pattern recognition*, pages 10867–10877, 2023. 1
- [10] Lei Huang, Weijiang Yu, Weitao Ma, Weihong Zhong, Zhangyin Feng, Haotian Wang, Qianglong Chen, Weihua Peng, Xiaocheng Feng, Bing Qin, et al. A survey on hallucination in large language models: Principles, taxonomy, challenges, and open questions. *ACM Transactions on Information Systems*, 43(2):1–55, 2025. 1
- [11] Qidong Huang, Xiaoyi Dong, Pan Zhang, Bin Wang, Conghui He, Jiaqi Wang, Dahua Lin, Weiming Zhang, and Nenghai Yu. Opera: Alleviating hallucination in multimodal large language models via over-trust penalty and retrospection-allocation. In *Proceedings of the IEEE/CVF Conference on Computer Vision and Pattern Recognition*, pages 13418–13427, 2024. 2, 4, 6, 1
- [12] Fushuo Huo, Wenchao Xu, Zhong Zhang, Haozhao Wang, Zhicheng Chen, and Peilin Zhao. Self-introspective decoding: Alleviating hallucinations for large vision-language models. In *The Thirteenth International Conference on Learning Representations, ICLR 2025, Singapore, April 24-28, 2025*. OpenReview.net, 2025. 2
- [13] Chaoya Jiang, Haiyang Xu, Mengfan Dong, Jiaying Chen, Wei Ye, Ming Yan, Qinghao Ye, Ji Zhang, Fei Huang, and Shikun Zhang. Hallucination augmented contrastive learning for multimodal large language model. In *Proceedings of the IEEE/CVF Conference on Computer Vision and Pattern Recognition*, pages 27036–27046, 2024. 1, 2
- [14] Zhangqi Jiang, Junkai Chen, Beier Zhu, Tingjin Luo, Yankun Shen, and Xu Yang. Devils in middle layers of large vision-language models: Interpreting, detecting and mitigating object hallucinations via attention lens. In *Proceedings of the IEEE/CVF Conference on Computer Vision and Pattern Recognition (CVPR)*, pages 25004–25014, 2025. 2, 6
- [15] Mingi Jung, Saehyung Lee, Eunji Kim, and Sungroh Yoon. Visual attention never fades: Selective progressive attention recalibration for detailed image captioning in multimodal large language models. In *Forty-second International Conference on Machine Learning*, 2025. 2, 6
- [16] Seil Kang, Jinyeong Kim, Junhyeok Kim, and Seong Jae Hwang. See what you are told: Visual attention sink in large multimodal models. In *The Thirteenth International Conference on Learning Representations*, 2025. 2
- [17] Sicong Leng, Hang Zhang, Guanzheng Chen, Xin Li, Shijian Lu, Chunyan Miao, and Lidong Bing. Mitigating object hallucinations in large vision-language models through visual contrastive decoding. In *Proceedings of the IEEE/CVF Conference on Computer Vision and Pattern Recognition*, pages 13872–13882, 2024. 2, 6
- [18] Dongxu Li, Junnan Li, Hung Le, Guangsen Wang, Silvio Savarese, and Steven CH Hoi. Lavis: A library for language-vision intelligence. *arXiv preprint arXiv:2209.09019*, 2022. 1, 6
- [19] Junnan Li, Dongxu Li, Silvio Savarese, and Steven Hoi. Blip-2: Bootstrapping language-image pre-training with frozen image encoders and large language models. In *International conference on machine learning*, pages 19730–19742. PMLR, 2023. 1
- [20] Yifan Li, Yifan Du, Kun Zhou, Jinpeng Wang, Wayne Xin Zhao, and Ji-Rong Wen. Evaluating object hallucination in large vision-language models. In *Proceedings of the 2023 Conference on Empirical Methods in Natural Language Processing*, pages 292–305, 2023. 1
- [21] Zhuowei Li, Haizhou Shi, Yunhe Gao, Di Liu, Zhenting Wang, Yuxiao Chen, Ting Liu, Long Zhao, Hao Wang, and Dimitris N Metaxas. The hidden life of tokens: Reducing

- hallucination of large vision-language models via visual information steering. *arXiv preprint arXiv:2502.03628*, 2025. [2](#)
- [22] Tian Liang, Yuetian Du, Jing Huang, Ming Kong, Luyuan Chen, Yadong Li, Siye Chen, and Qiang Zhu. Mole: Decoding by mixture of layer experts alleviates hallucination in large vision-language models. In *Proceedings of the AAAI Conference on Artificial Intelligence*, pages 18684–18692, 2025. [2](#)
- [23] Haotian Liu, Chunyuan Li, Yuheng Li, and Yong Jae Lee. Improved baselines with visual instruction tuning. In *Proceedings of the IEEE/CVF conference on computer vision and pattern recognition*, pages 26296–26306, 2024. [1](#), [6](#)
- [24] Hanchao Liu, Wenyuan Xue, Yifei Chen, Dapeng Chen, Xiutian Zhao, Ke Wang, Liping Hou, Rongjun Li, and Wei Peng. A survey on hallucination in large vision-language models. *arXiv preprint arXiv:2402.00253*, 2024. [1](#)
- [25] Shi Liu, Kecheng Zheng, and Wei Chen. Paying more attention to image: A training-free method for alleviating hallucination in lvlms. In *Proceedings of the European Conference on Computer Vision (ECCV)*, pages 125–140, 2024. [2](#), [6](#)
- [26] Xinyu Lyu, Beita Chen, Lianli Gao, Hengtao Shen, and Jingkuan Song. Alleviating hallucinations in large vision-language models through hallucination-induced optimization. *Advances in Neural Information Processing Systems*, 37:122811–122832, 2024. [2](#)
- [27] OpenAI. Gpt-4 technical report. *CoRR*, abs/2303.08774, 2023. [6](#), [2](#)
- [28] Yeji Park, Deokyeon Lee, Junsuk Choe, and Buru Chang. Convis: Contrastive decoding with hallucination visualization for mitigating hallucinations in multimodal large language models. In *Proceedings of the AAAI Conference on Artificial Intelligence*, pages 6434–6442, 2025. [2](#)
- [29] Anna Rohrbach, Lisa Anne Hendricks, Kaylee Burns, Trevor Darrell, and Kate Saenko. Object hallucination in image captioning. In *Proceedings of the 2018 Conference on Empirical Methods in Natural Language Processing*, pages 4035–4045, Brussels, Belgium, 2018. Association for Computational Linguistics. [1](#), [6](#), [2](#)
- [30] Fengyuan Sun, Hui Chen, Xinhao Xu, Dandan Zheng, Jingdong Chen, Jun Zhou, Jungong Han, and Guiguang Ding. Prunehal: Reducing hallucinations in multi-modal large language models through adaptive kv cache pruning. *arXiv preprint arXiv:2510.19183*, 2025. [2](#)
- [31] Qingfeng Sun, Yujing Wang, Can Xu, Kai Zheng, Yaming Yang, Huang Hu, Fei Xu, Jessica Zhang, Xiubo Geng, and Daxin Jiang. Multimodal dialogue response generation. In *Proceedings of the 60th Annual Meeting of the Association for Computational Linguistics (Volume 1: Long Papers)*, *ACL 2022, Dublin, Ireland, May 22-27, 2022*, pages 2854–2866. Association for Computational Linguistics, 2022. [1](#)
- [32] Feilong Tang, Zile Huang, Chengzhi Liu, Qiang Sun, Harry Yang, and Ser-Nam Lim. Intervening anchor token: Decoding strategy in alleviating hallucinations for mllms. In *The Thirteenth International Conference on Learning Representations, ICLR 2025, Singapore, April 24-28, 2025*. OpenReview.net, 2025. [2](#)
- [33] Feilong Tang, Chengzhi Liu, Zhongxing Xu, Ming Hu, Zile Huang, Haochen Xue, Ziyang Chen, Zelin Peng, Zhiwei Yang, Sijin Zhou, et al. Seeing far and clearly: Mitigating hallucinations in mllms with attention causal decoding. In *Proceedings of the Computer Vision and Pattern Recognition Conference*, pages 26147–26159, 2025. [2](#)
- [34] Chongjun Tu, Peng Ye, Dongzhan Zhou, Lei Bai, Gang Yu, Tao Chen, and Wanli Ouyang. Attention reallocation: Towards zero-cost and controllable hallucination mitigation of mllms. *CoRR*, abs/2503.08342, 2025. [2](#)
- [35] Junyang Wang, Yuhang Wang, Guohai Xu, Jing Zhang, Yukai Gu, Haitao Jia, Ming Yan, Ji Zhang, and Jitao Sang. An llm-free multi-dimensional benchmark for mllms hallucination evaluation. *arXiv preprint arXiv:2311.07397*, 2023. [6](#), [2](#)
- [36] Yuanchen Wu, Lu Zhang, Hang Yao, Junlong Du, Ke Yan, Shouhong Ding, Yunsheng Wu, and Xiaoqiang Li. Antidote: A unified framework for mitigating lvlm hallucinations in counterfactual presupposition and object perception. In *Proceedings of the Computer Vision and Pattern Recognition Conference*, pages 14646–14656, 2025. [2](#)
- [37] Guangxuan Xiao, Yuandong Tian, Beidi Chen, Song Han, and Mike Lewis. Efficient streaming language models with attention sinks. In *The Twelfth International Conference on Learning Representations, ICLR 2024, Vienna, Austria, May 7-11, 2024*. OpenReview.net, 2024. [2](#)
- [38] Wenyi Xiao, Ziwei Huang, Leilei Gan, Wangui He, Haoyuan Li, Zhelun Yu, Fangxun Shu, Hao Jiang, and Linchao Zhu. Detecting and mitigating hallucination in large vision language models via fine-grained ai feedback. In *Proceedings of the AAAI Conference on Artificial Intelligence*, pages 25543–25551, 2025. [2](#)
- [39] Xinhao Xu, Hui Chen, Mengyao Lyu, Sicheng Zhao, Yizhe Xiong, Zijia Lin, Jungong Han, and Guiguang Ding. Mitigating hallucinations in multi-modal large language models via image token attention-guided decoding. In *Proceedings of the 2025 Conference of the Nations of the Americas Chapter of the Association for Computational Linguistics: Human Language Technologies (Volume 1: Long Papers)*, pages 1571–1590, Albuquerque, New Mexico, 2025. Association for Computational Linguistics. [2](#)
- [40] Tianyun Yang, Ziniu Li, Juan Cao, and Chang Xu. Understanding and mitigating hallucination in large vision-language models via modular attribution and intervention. In *The Thirteenth International Conference on Learning Representations, ICLR 2025, Singapore, April 24-28, 2025*. OpenReview.net, 2025. [2](#)
- [41] Zhihe Yang, Xufang Luo, Dongqi Han, Yunjian Xu, and Dongsheng Li. Mitigating hallucinations in large vision-language models via dpo: On-policy data hold the key. In *Proceedings of the Computer Vision and Pattern Recognition Conference*, pages 10610–10620, 2025. [2](#)
- [42] Yiyang Zhou, Chenhang Cui, Rafael Rafailov, Chelsea Finn, and Huaxiu Yao. Aligning modalities in vision large language models via preference fine-tuning. *arXiv preprint arXiv:2402.11411*, 2024. [2](#)
- [43] Deyao Zhu, Jun Chen, Xiaoqian Shen, Xiang Li, and Mohamed Elhoseiny. Minigt-4: Enhancing vision-language

understanding with advanced large language models. In *The Twelfth International Conference on Learning Representations, ICLR 2024, Vienna, Austria, May 7-11, 2024*. Open-Review.net, 2024. [1](#), [6](#)

# KVSmooth: Mitigating Hallucination in Multi-modal Large Language Models through Key-Value Smoothing

## Supplementary Material

### A. The Detailed Derivation of EMA Smoothing on Hidden States

During inference, this growth manifests as increasingly large token-wise logit moments: the model state oscillates violently, drifts away from the visual prior, and deviates from the true image information through sudden jumps. To keep the decoding trajectory ideally smooth, we formalize the following hypothesis:

$$h_t = h_{t-1} + \epsilon_t, \epsilon_t \sim N(0, \sigma_p^2). \quad (16)$$

Consequently, the transition prior is

$$P(h_t|h_{t-1}) = N(h_t; h_{t-1}, \sigma_p^2) \propto \exp\left(-\frac{1}{2\sigma_p^2} \|h_t - h_{t-1}\|^2\right). \quad (17)$$

Under this prior, the maximum-a-posteriori (MAP) estimate of  $h_t$  is given by

$$\hat{h}_t = \operatorname{argmax}_{h_t} \left[ \underbrace{\log P(o_t|h_t)}_{\text{likelihood}} + \underbrace{\log P(h_t|h_{t-1})}_{\text{smoothed prior}} \right], \quad (18)$$

where  $o_t$  denotes the raw hidden state observed at step  $t$ . Assuming both terms are Gaussian, we have

$$P(o_t|h_t) \propto \exp\left(-\frac{1}{2\sigma_o^2} \|o_t - h_t\|^2\right), \quad (19)$$

$$P(h_t|h_{t-1}) \propto \exp\left(-\frac{1}{2\sigma_p^2} \|h_t - h_{t-1}\|^2\right). \quad (20)$$

Substituting (19) and (20) into (18) yields

$$\hat{h}_t = \operatorname{argmax}_{h_t} \left[ -\frac{1}{2\sigma_o^2} \|o_t - h_t\|^2 - \frac{1}{2\sigma_p^2} \|h_t - h_{t-1}\|^2 \right]. \quad (21)$$

Taking the derivative of (21) with respect to  $h_t$  and setting it to zero, we obtain:

$$\frac{\partial}{\partial h_t} \left[ -\frac{1}{2\sigma_o^2} \|o_t - h_t\|^2 - \frac{1}{2\sigma_p^2} \|h_t - h_{t-1}\|^2 \right] = 0 \quad (22)$$

$$\frac{1}{\sigma_o^2} (o_t - h_t) - \frac{1}{\sigma_p^2} (h_t - h_{t-1}) = 0.$$

Solving for  $\hat{h}_t$ , we obtain

$$\hat{h}_t = \frac{\sigma_p^2}{\sigma_p^2 + \sigma_o^2} o_t + \frac{\sigma_o^2}{\sigma_p^2 + \sigma_o^2} h_{t-1}. \quad (23)$$

Defining

$$\lambda_t = \frac{\sigma_o^2}{\sigma_p^2 + \sigma_o^2}, \quad (24)$$

the estimate reduces to the exponential moving average (EMA) form

$$\hat{h}_t = (1 - \lambda_t) o_t + \lambda_t h_{t-1}. \quad (25)$$

Thus, when the likelihood is Gaussian in  $h_t$ , the MAP estimator coincides exactly with an exponential moving average.

### B. Benchmark Details

We briefly describe the four benchmarks used for evaluation:

**CHAIR.** CHAIR [29] is a classic benchmark for measuring **object hallucination** in image captioning tasks. It defines two key metrics:

- **CHAIR<sub>S</sub>** (Sentence-level Hallucination) — the proportion of captions that contain at least one hallucinated object.
- **F<sub>1</sub>** — a balanced measure reflecting both the accuracy and completeness of generated captions. In CHAIR, *precision* quantifies the proportion of generated objects that correctly appear in the ground-truth annotations, while *recall* measures how many ground-truth objects are successfully mentioned in the generated captions. The F<sub>1</sub> score captures the overall trade-off between these two factors.

In this work, following [11], we randomly sample 500 images from the COCO 2014 validation set and prompt the LVLMs with “Please describe the image in detail.” The maximum output length is set to 512 tokens.

**OPOPE.** OPOPE [4] extends POPE [20] by transforming its interactive yes/no polling mechanism into an **offline evaluation**. It retains POPE’s three sampling strategies — *random*, *popular*, and *adversarial* — but checks whether sampled positive and negative objects appear in the model-generated image descriptions instead of interacting with the model. Following [4], we report the following metrics:

- **Accuracy** — overall correctness of object presence identification.
- **Precision** — proportion of correctly identified positive objects among all predicted positives.

- $F_{\beta=0.2}$ — defined as

$$F_{\beta} = (1 + \beta^2) \frac{\text{Precision} \cdot \text{Recall}}{\beta^2 \cdot \text{Precision} + \text{Recall}}, \quad \beta = 0.2,$$

which reduces the impact of false negatives following [4]. All reported numbers are averaged over the three sampling methods (random, popular, and adversarial).

**AMBER.** AMBER [35] is a benchmark for evaluating hallucinations in vision-language models from both generative and discriminative perspectives. In this work, we focus on the generative task setting to assess model performance. The dataset encompasses 14 major object categories, featuring a balanced distribution that mitigates the significant long-tail issue. Compared to existing benchmarks, AMBER extends coverage to categories such as Nature, Architecture, and Street View, and provides richer annotations in others—for example, the Fruit category includes over a dozen common fruits, whereas prior datasets only cover three types.

Following [35], we adopt four metrics for evaluation:

- **CHAIR** — object hallucination rate in responses.
- **Cover** — proportion of objects mentioned in the response relative to annotated objects, reflecting faithful object coverage.
- **Hal** — proportion of responses containing hallucinations.
- **Cog** — measures the extent to which hallucinated objects align with common human cognitive biases.

**Object HalBench.** Object HalBench (ObjHal) [29] is a diverse benchmark for evaluating **object hallucination robustness** under different prompt styles. It assesses models on 300 image–text pairs using eight varied prompts, providing a stable and comprehensive evaluation. Here, GPT-4 [27] is used to extract visible objects from the captions generated by the model.

The benchmark reports four main metrics:

- **CHAIR<sub>S</sub>** — Image-level hallucination rate: proportion of images containing at least one hallucinated object.
- **CHAIR<sub>SR</sub>** — Similar to CHAIR<sub>S</sub> but excludes sentences without any object words; measures hallucination among sentences containing at least one MSCOCO object word.
- **CHAIR<sub>I</sub>** — Proportion of hallucinated objects among all generated object words.
- **CoCoNum** — Number of captions containing at least one COCO object.

### C. Efficiency Comparisons

To further assess the computational efficiency and resource usage of our approach, we compare its average per-caption

Table 5. Comparison of token generation efficiency and resource usage across different methods on LLaVA-1.5 (CHAIR benchmark). Our method delivers faster inference and lower memory cost than other training-free hallucination mitigation methods.

Method	Avg. Time (s/caption)	Peak Memory (MB)	Latency (ms/token)	Throughput (token/s)
Baseline	<b>3.36</b>	<u>14629.21</u>	<b>31.24</b>	<b>32.06</b>
PAI	6.68	15003.25	56.44	17.73
OPERA	34.62	19531.97	313.78	3.43
SPARC	4.13	14644.61	35.20	28.44
Ours	<u>3.61</u>	<b>14625.06</b>	<u>34.33</u>	<u>29.18</u>

inference time, token-level latency, throughput, and memory consumption with several representative hallucination mitigation methods, as summarized in Table 5.

As illustrated in the table, our method achieves a favorable trade-off between performance and efficiency. It maintains a comparable runtime and memory footprint to the baseline model while significantly reducing hallucinations. Notably, compared with more complex attention redistribution approaches such as SPARC and PAI, our approach requires substantially less computation time and memory overhead. This demonstrates that our smoothing mechanism is lightweight and can be seamlessly integrated into existing vision-language models without compromising efficiency.

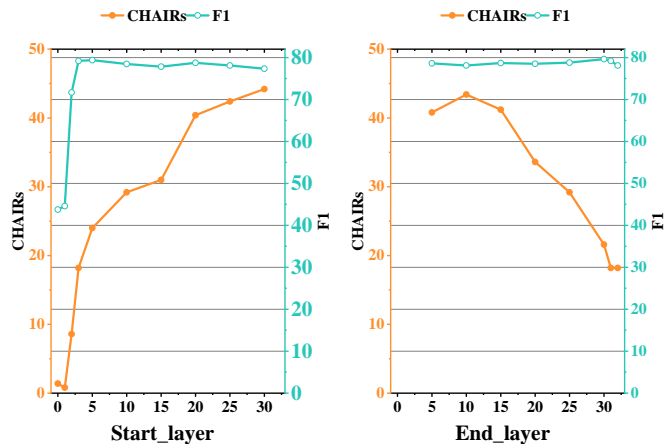


Figure 6. Sensitivity analysis of the layer range for KVSmooth on LLaVA-1.5 (CHAIR benchmark). Left: sensitivity to start layer ( $L_{\text{start}}$ ); Right: sensitivity to end layer ( $L_{\text{end}}$ ).

### D. Parameter Sensitivity

To evaluate the robustness of our approach, we conduct a sensitivity analysis on key hyperparameters across three MLLMs, including the EMA decay rate  $\lambda_{\text{ref}}$ , which determines the strength of the smoothing effect, and the start

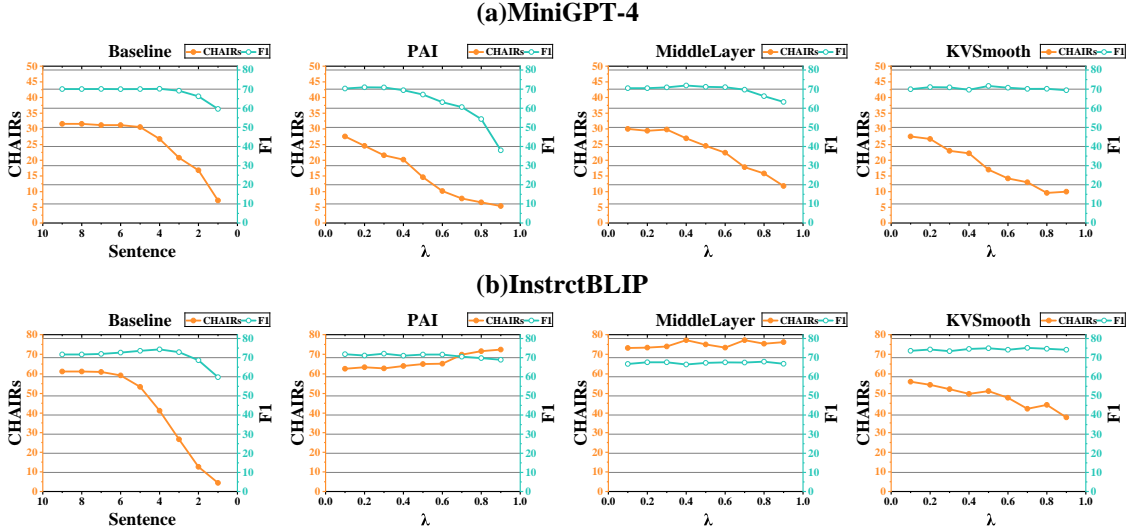


Figure 7. Sensitivity analysis of the hyperparameter  $\lambda_{\text{ref}}$  for KVSmooth based on MiniGPT-4 (a) and InstructBLIP (b) and comparisons of four methods in terms of the CHAIR<sub>S</sub>-F<sub>1</sub> trade-off (CHAIR benchmark). Larger values of  $\lambda_{\text{ref}}$  lead to stronger smoothing and more effective hallucination mitigation. Moreover, our method consistently maintains a favorable balance between precision and recall: it reduces hallucinations while preserving a high F<sub>1</sub> score, demonstrating diverse and reliable object coverage across different smoothing strengths.

layer ( $L_{\text{start}}$ ) and end layer ( $L_{\text{end}}$ ), which define the range of layers where EMA is applied. We vary each parameter while keeping the others fixed to examine its influence on overall performance.

### D.1. Effect of the Reference Smoothing Coefficient

$\lambda_{\text{ref}}$

Specifically, we analyze the influence of the decay threshold range by varying  $\lambda_{\text{ref}}$  and evaluating KVSmooth on the CHAIR benchmark, measuring both CHAIR<sub>S</sub> and F<sub>1</sub> metrics. As shown in Figure 5 and Figure 7, the CHAIR<sub>S</sub> score consistently decreases as  $\lambda_{\text{ref}}$  increases, while the F<sub>1</sub> score remains nearly unchanged. This indicates that a larger  $\lambda_{\text{ref}}$  leads to stronger smoothing effects and more effective hallucination mitigation. Moreover, despite enhanced hallucination suppression, KVSmooth maintains a stable balance between precision and recall, demonstrating robustness across different smoothing strengths.

### D.2. Effect of Start and End Layers ( $L_{\text{start}}, L_{\text{end}}$ ).

To determine the optimal layer range for applying EMA updates, we conduct a two-dimensional layer sweep. First, we fix the end layer  $L_{\text{end}}$  at 31 and vary the start layer  $L_{\text{start}}$  from 0 to 30. Then, we fix  $L_{\text{start}}$  at 3 and vary  $L_{\text{end}}$  from 5 to 32. As shown in Figure 6, CHAIR<sub>S</sub> decreases gradually as more layers are included in the EMA updates, demonstrating stronger hallucination suppression. However, applying EMA at the very early (0–2) or final (32) layers causes a noticeable drop in F<sub>1</sub>, indicating that excessive smoothing

in these regions impairs the model’s ability to represent real objects and degrades caption quality.

## E. The Algorithm of KVSmooth

In this section, we present the full algorithmic details of KVSmooth. The algorithm consists of two components: **Algorithm 1: EMA Smoothing on KV-Cache**, corresponding to Section 4.3 (*The Final KVSmooth Method*); and **Algorithm 2: Attention Forward with Adaptive EMA Smoothing**, corresponding to Section 3.1 (*Formulation of MLLMs Generation*) and Section 4.2 (*Entropy-Guided Coefficient Adaptation*).

---

### Algorithm 1: EMA Smoothing on KV-Cache

---

**Input:** KV-cache  $C_t^l = (K_{1:t}^{(l,h)}, V_{1:t}^{(l,h)})_{h=1}^H$ , smoothing coefficient  $\tilde{\lambda}_t^l$

**Output:** Smoothed KV-cache  $C_t^l = (K_{1:t}^{(l,h)}, V_{1:t}^{(l,h)})_{h=1}^H$

1. EMA update for each head  $h$ :

$$\hat{K}_t^{(l,h)} \leftarrow (1 - \tilde{\lambda}_t^l) K_t^{(l,h)} + \tilde{\lambda}_t^l K_{t-1}^{(l,h)},$$

$$\hat{V}_t^{(l,h)} \leftarrow (1 - \tilde{\lambda}_t^l) V_t^{(l,h)} + \tilde{\lambda}_t^l V_{t-1}^{(l,h)}.$$

2. Update smoothed cache:

$$K_t^{(l,h)} \leftarrow \hat{K}_t^{(l,h)}, \quad V_t^{(l,h)} \leftarrow \hat{V}_t^{(l,h)}.$$

**return**  $C_t^l$

---

---

**Algorithm 2:** Attention Forward with Adaptive EMA Smoothing

---

**Input:** Hidden state  $h_t$ , mask  $M$ , KV-cache  $C_{t-1}^l$ , entropy queue  $S^l$ , reference coefficient  $\lambda_{\text{ref}}$

**Output:** Updated hidden state  $h_t^l$ , attention weights  $\alpha_t^{(l,h)}$ , KV-cache  $C_t^l$ , entropy queue  $S^l$

1. **Compute Q, K, V for each head  $h$ :**

$$Q_t^{(l,h)} = h_t W_Q^{(l,h)}, \quad K_t^{(l,h)} = h_t W_K^{(l,h)}, \quad V_t^{(l,h)} = h_t W_V^{(l,h)}.$$

2. **Update KV-cache:** Append  $(K_t^{(l,h)}, V_t^{(l,h)})$  to  $C_{t-1}^l$  to obtain  $C_t^l$ .

3. **Compute attention scores:**

$$A_{t,j}^{(l,h)} = \frac{(Q_t^{(l,h)})^\top K_j^{(l,h)}}{\sqrt{d}} + M_{t,j}.$$

4. **Compute attention weights and row-entropy:**

$$\alpha_{t,j}^{(l,h)} = \text{Softmax}_j(A_{t,j}^{(l,h)}),$$
$$z_{t,j}^l = -\frac{1}{H} \sum_{h=0}^{H-1} \sum_{i=0}^{L-1} \alpha_{i,j}^{(l,h)} \log(\alpha_{i,j}^{(l,h)} + \varepsilon).$$

Insert  $z_{t,j}^l$  into the entropy queue  $S^l$ .

5. **Determine adaptive smoothing coefficient:** Compute the percentile rank  $k$  of  $z_{t,j}^l$  in  $S^l$ .

$$\hat{\lambda}_t^l = k/|S^l|,$$
$$\tilde{\lambda}_t^l = \text{clip}(\hat{\lambda}_t^l, \lambda_{\text{ref}} - 0.2, \lambda_{\text{ref}} + 0.2).$$

6. **Compute attention output:**

$$o_t^{(l,h)} = \sum_{j=0}^{L-1} \alpha_{t,j}^{(l,h)} V_j^{(l,h)},$$
$$h_t^l = \text{Concat}_h(o_t^{(l,h)}) W_O^l.$$

7. **Apply EMA smoothing for each head:**

$$(K_{1:t}^{(l,h)}, V_{1:t}^{(l,h)})_{h=1}^H \leftarrow \text{EMASmoothingon}((K_{1:t}^{(l,h)}, V_{1:t}^{(l,h)})_{h=1}^H, \tilde{\lambda}_t^l).$$

**return**  $h_t^l, \alpha_t^{(l,h)}, C_t^l, S^l$

---

## F. Qualitative Results

To illustrate the effectiveness of KVSmooth, we show representative examples where **orange** denotes baseline hallucinations and **cyan** denotes the corrections by KVSmooth, demonstrating its ability to fix factual errors while preserving coherence.



**Baseline**

The image features a large, shiny orange motorcycle on display at a show. The motorcycle is prominently positioned in the center of the scene, drawing attention to its unique design. There are several people surrounding the motorcycle, admiring and observing it. Some of them are standing closer to the motorcycle, while others are positioned further away. In addition to the motorcycle, there are a few bottles scattered around the scene, possibly indicating that the event is a casual gathering or a social event.

**KVSmooth**

The image features a large, shiny orange motorcycle on display at a show, likely an exhibition or a convention. The motorcycle is prominently displayed, occupying a significant portion of the scene. There are several people surrounding the motorcycle, with some standing closer to the front and others further back. In addition to the main motorcycle, there are a few other motorcycles visible in the background, indicating that this event showcases various motorcycles. The scene captures the attention of the visitors, as they gather around to admire the impressive display.



**Baseline**

The image features a man wearing a coat and holding a sandwich in his hand. He appears to be eating the sandwich while standing outside. There are several other people in the scene, some of them carrying backpacks and handbags. In the background, there are a few cars parked, and a bench can be seen nearby. The scene seems to be a busy outdoor area with people going about their daily activities.

**KVSmooth**

The image features a man wearing a tan jacket, standing outside in the snow. He is holding a sandwich in his hand, likely enjoying a bite of his meal. The man appears to be focused on his food, possibly taking a break from the cold weather. There are several other people in the scene, some of them standing in the background, possibly walking by or engaging in their own activities. A backpack can be seen in the background, possibly belonging to one of the people in the scene.



**Baseline**

The image features two women in a room, playing a video game together. One woman is standing and holding a Wii remote, while the other woman is sitting on a bed, also holding a Wii remote. They appear to be enjoying their time together, possibly playing a game like Wii Sports. The room has a couch in the background, and a laptop is placed on the bed. There are also two potted plants in the room, one near the couch and the other closer to the standing woman. The scene captures a fun and interactive moment between the two women.

**KVSmooth**

The image features two women in a room, with one woman standing and another person sitting on a bed. The woman standing is holding a Wii remote, likely playing a video game. The woman on the bed is sitting on a bed, watching and possibly observing the gameplay. The room appears to be a cozy living space, with a couch in the background and a laptop placed on a surface nearby. The scene suggests that the two women are enjoying a fun and interactive gaming session together.

Figure 8. Qualitative results on LLaVA-1.5: baseline (w/o KVSmooth) vs. KVSmooth.



#### Baseline

The image shows a large clock hanging from a pole on the side of a building. The clock has a black face and white numbers, and is surrounded by green leaves. The building behind the clock is tall and made of stone. There are several signs on the pole, including a street sign pointing to the right and a sign for a business on the left. The sky is clear and blue, and there are a few clouds in the distance.

#### KVSmooth

The image shows a large clock hanging from a pole on the side of a building. The clock has a black face and roman numerals. The clock is surrounded by street signs pointing in different directions. The building behind the clock is a tall, modern building with many windows and a large, ornate facade. The sky is clear and blue with a few clouds in the sky.



#### Baseline

The image shows a long train traveling down a railroad track. The train is made up of several cars, each carrying different types of cargo. The train appears to be carrying a mix of goods, including grains, minerals, and other materials. The track is lined with trees and other vegetation, and there is a clear blue sky in the background. The image is taken from a high angle, looking down on the train as it moves along the track.

#### KVSmooth

The image shows a long train traveling down a railroad track. The train is yellow and red, with yellow cargo cars. There are trees in the background. The image is taken from above, looking down on the train as it goes along the track.



#### Baseline

The image shows a group of people in a living room. There is a cake on a table in front of them, and they are all wearing party clothes. One person is holding a knife and is about to cut the cake. Another person is holding a glass of champagne. The room is dimly lit, and there are several pieces of furniture in the background.

#### KVSmooth

The image shows a group of people in a living room. There is a young woman standing in front of a cake on a table, holding a knife in her hand. She is wearing a green shirt and jeans. There is a man standing behind her, watching her. The room is dimly lit and there is a television in the background.

Figure 9. Qualitative results on MiniGPT-4: baseline (w/o KVSmooth) vs. KVSmooth.



**Baseline**

The image features a young woman wearing a pink sweater and a skirt standing in a kitchen. She is posing for the camera, and her hair is styled in a ponytail. The kitchen is equipped with various appliances, including a sink, an oven, and a refrigerator. There are also several bottles and bowls placed around the kitchen, suggesting that the woman is preparing food or drinks. In addition to the kitchen appliances and food items, there are several other objects scattered throughout the scene, including a chair, a table, and a book. The overall atmosphere of the image is lively and welcoming. The woman's ponytail and the appliances in the kitchen give the impression of a cozy and functional space. The presence of the book suggests that the woman may be engaging in some form of learning or entertainment. Overall, the scene captures a young woman in a cheerful and productive kitchen setting.

**KVSmooth**

The image features a young woman standing in a kitchen, wearing a pink sweater and a skirt. She is holding her hand on her hip and posing for the camera. In the background, there are several cabinets visible, including one on the left side of the room and another on the right side. Various bottles can be seen scattered around the kitchen, with some located near the cabinets and others placed on the countertops. There are also two bowls present in the scene, one on the countertop to the left and another on the countertop to the right. The overall atmosphere of the kitchen appears to be cozy and inviting.



**Baseline**

The image shows a luxurious bedroom with a large bed in the center. The bed is adorned with two folded towels that resemble elephants, sitting on top of the bed as if they were guarding the room. There are several lamps placed around the bed, providing ample lighting for the space. A chair can be seen on the right side of the bed, and a second chair is positioned on the left side. In addition to the towels and lamps, there are several other items in the room, including a book placed on the bed, a lamp on the left side, and a second book placed on the right side. The room appears to be well-appointed and inviting, with a comfortable atmosphere for guests to relax and enjoy their stay.

**KVSmooth**

The image shows a luxurious bedroom with a large, neatly made bed. Two folded towels are placed on the bed in the shape of two elephants, creating an eye-catching display. There are several lamps positioned around the room, including one on each side of the bed and multiple cushions can be seen scattered across the surface of the bed. A chair is also present in the room, placed close to the bed. The arrangement of the bedding and decorations creates a cozy and inviting atmosphere for guests or visitors to enjoy. The towel elephant display adds a playful touch to the otherwise elegant bed setup, making it a unique and memorable feature of the room. Overall, the bedroom appears to be well-appointed and welcoming.



**Baseline**

The image features a table set up with a white plate containing a sandwich, which appears to be a grilled cheese sandwich. The sandwich is placed on top of the plate and is surrounded by various ingredients, such as tomatoes and lettuce. There are two bottles of juice on the table, one on the left side and the other on the right side. A glass of punch is also visible, placed in front of the sandwich. A knife is placed near the plate, likely for cutting the sandwich. A bowl is situated next to the plate, possibly containing additional ingredients or condiments. In the background, there is a refrigerator and a sink, suggesting that this is a kitchen setting. Overall, the scene showcases a well-prepared and appetizing meal.

**KVSmooth**

The image features a table set up with a white plate containing a sandwich, a glass of juice, and a bottle of water. The plate is placed on a countertop, and there are two bottles visible in the background. One bottle is located on the left side of the image, while the other is on the right side. The plate is adorned with various vegetables, including tomatoes and lettuce. The sandwich appears to be a hearty and flavorful meal. The table also includes a bottle of juice, which is likely to complement the sandwich. The setup suggests that the person enjoying the meal is taking a break from their daily routine. Overall, the scene showcases a well-prepared and satisfying meal.

Figure 10. Qualitative results on InstructBLIP: baseline (w/o KVSmooth) vs. KVSmooth.